Mineralogy and Petrology (2003) 78: 1–20
DOI 10.1007/s00710-002-0203-6

Mineralogy and Petrology
Printed in Austria

Himalayan magmatism and porphyry copper–molybdenum mineralization in the Yulong ore belt, East Tibet

X. X. Gu[1,2], **J. X. Tang**[2], **C. S. Wang**[2], **J. P. Chen**[2], and **B. B. He**[2]

[1] Institute of Geochemistry, Chinese Academy of Sciences, Guiyang, P.R. China
[2] Chengdu University of Technology, Chengdu, P.R. China

Received August 29, 2001; revised version accepted May 1, 2002
Published online: November 29, 2002;
Editorial handling: K. Stűwe

Summary

The NW–SE-trending Yulong porphyry Cu–Mo ore belt, situated in the Sanjiang area of eastern Tibet, is approximately 400 km long and 35 to 70 km wide. Complex tectonic and magmatic processes during the Himalayan epoch have given rise to favorable conditions for porphyry-type Cu–Mo mineralization.

Porphyry masses of the Himalayan epoch in the Yulong ore belt are distributed in groups along regional NW–SE striking tectonic lineaments. They were emplaced mainly into Triassic and Lower Permian sedimentary-volcanic rocks. K–Ar und U–Pb isotopic datings give an intrusion age range of 57–26 Ma. The porphyries are mainly of biotite monzogranitic and biotite syenogranitic compositions. Geological and geochemical data indicate that the various porphyritic intrusions in the belt had a common or similar magma source, are metaluminous to peraluminous, Nb–Y–Ba-depleted, I-type granitoids, and belong to the high-K calc-alkaline series.

Within the Yulong subvolcanic belt a number of porphyry stocks bear typical porphyry type Cu–Mo alteration and mineralization. The most prominent porphyry Co–Mo deposits include Yulong, Malasongduo, Duoxiasongduo, Mangzong and Zhanaga, of which Yulong is one of the largest porphyry Cu (Mo) deposits in China with approximately 8×10^6 tons of contained Cu metal. Hydrothermal alteration at Yulong developed around a biotite–monzogranitic porphyry stock that was emplaced within Upper Triassic limestone, siltstone and mudstone. The earliest alteration was due to the effects of contact metamorphism of the country rocks and alkali metasomatism (potassic alteration) within and around the porphyry body. The alteration of this stage was accompanied by a small amount of disseminated and veinlet Cu–Mo sulfide mineralization. Later alteration–mineralization zones form more or less concentric shells

around the potassic zone, around which are distributed a phyllic or quartz–sericite–pyrite zone, a silicification and argillic zone, and a propylitic zone.

Fluid inclusion data indicate that three types of fluids were involved in the alteration–mineralization processes: (1) early high temperature (660–420 °C) and high salinity (30–51 wt% NaCl equiv) fluids responsible for the potassic alteration and the earliest disseminated and/or veinlet Cu–Mo sulfide mineralization; (2) intermediate unmixed fluids corresponding to phyllic alteration and most Cu–Mo sulfide mineralization, with salinities of 30–50 wt% NaCl equiv and homogenization temperatures of 460–280 °C; and (3) late low to moderate temperature (300–160 °C) and low salinity (6–13 wt% NaCl equiv) fluids responsible for argillic and propylitic alteration. Hydrogen and oxygen isotopic studies show that the early hydrothermal fluids are of magmatic origin and were succeeded by increasing amounts of meteoric-derived convective waters. Sulfur isotopes also indicate a magmatic source for the sulfur in the early sulfide mineralization, with the increasing addition of sedimentary sulfur outward from the porphyry stock.

Introduction

There are two important porphyry copper–molybdenum metallogenic belts in the Tethys-Himalayan tectonic domain in western China, e.g., the W–E-trending Gangdise plutonic–volcanic arc belt and the NW–SE-trending Yulong porphyry metallogenic belt. The former resulted from the subduction of the Tethyan oceanic crust beneath the Lhasa block during the late Jurassic to Cretaceous and hosts a large number of porphyry Cu–Mo polymetallic deposits and prospects (*Gu* et al., 2000). The latter is a Mesozoic orogenic belt that was formed by the westward subduction of the Paleo-Tethyan oceanic crust beneath the Changdu-Simao block along the Jinshajiang suture zone during late Triassic time and was reactivated during the Himalayan orogeny (*Ma*, 1990; *Tang* and *Luo*, 1995). The porphyry Cu–Mo deposits of the Yulong belt are spatially and temporally related to discrete, shallowly emplaced, multiphase complexes of intermediate to felsic intrusions formed during the Himalayan orogeny.

Since the discovery of the Yulong Cu–Mo deposit in the late 1960s, extensive exploration in the Yulong porphyry belt has led to discovery of numerous deposits and prospects that have many features in common with Yulong and other porphyry-type Cu–Mo deposits in the world. Very little, however, has been described about these Chinese porphyry deposits in the Western literature. The major purpose of this paper is to document and interpret the tectonic setting, petrology, geochemistry and alteration–mineralization styles of the porphyry systems in the Yulong belt.

Regional geologic setting

The Yulong porphyry metallogenic belt, located in the Sanjiang area of eastern Tibet, is approximately 400 km long and 35 to 70 km wide. Tectonically, it is situated in a complex region where the Yangtze block, Indian plate and a number of smaller plates interact and collide (Fig. 1). The Qiangtang-Changdu microcontinent sandwiched between the Jinshajiang and Lancangjiang sutures comprises an eastern continental island arc and a western back arc basin. The Yulong belt

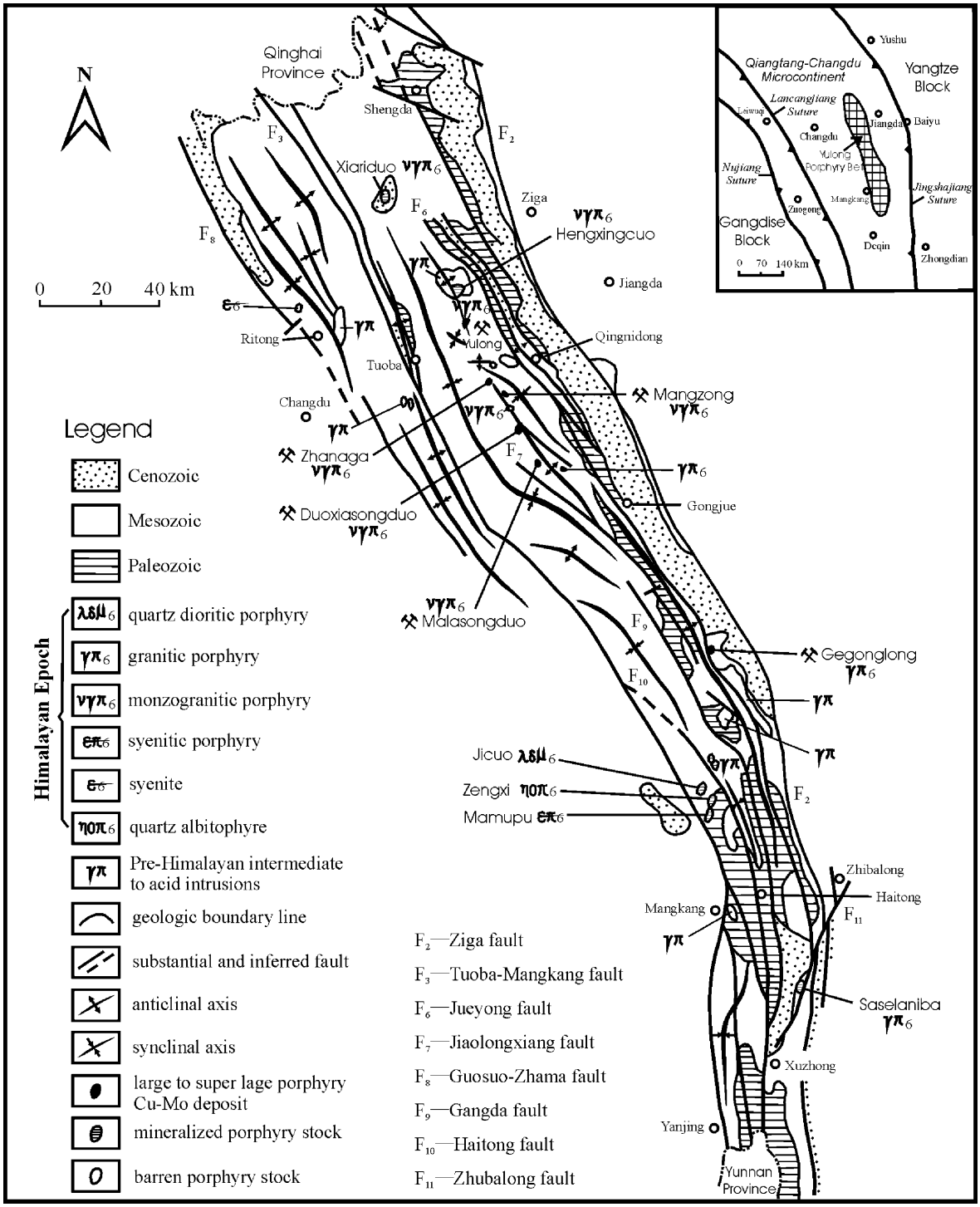

Fig. 1. Simplified geologic map of the Yulong porphyry ore belt (modified after *Tang* and *Luo*, 1995) with an inset showing the simplified plate tectonic features of East Tibet

constitutes the western part of the continental island arc. Westward subduction of the Paleo-Tethyan oceanic crust beneath the Qiangtang-Changdu microcontinent along the Jinshajiang suture zone during the late Permian to Triassic caused alkaline, calc-alkaline and tholeiitic volcanic activity (*Hao* and *Yu*, 1983; *Zhang* et al., 1983). Continent–continent collision between the Indian plate and Eurasia during the Himalayan orogeny triggered the reactivation of the Paleo-Tethyan subduction zone and resulted in the extensive emplacement of subvolcanic intrusions, including the productive porphyries of the Yulong belt.

The Yulong belt shown in Fig. 1 is tectonically characterized by a series of NW–SE-trending faults and folds. Porphyries commonly occur along hinges of antiforms. The oldest sedimentary rocks exposed are Lower Ordovician sandstone, slate and phyllite with intercalations of marble. They are unconformably overlain by a 4000–4500 m thick sequence of Devonian to Permian marine carbonates with 400 m of andesitic volcanic rocks in the uppermost part of the Upper Permian. Unconformably overlying these is the Lower Triassic Malasongduo Formation, which ranges from 500 to 3500 m in thickness and consists predominantly of dacitic to rhyolitic lava and pyroclastic rocks interbedded with black shale and sandstone. This formation is in turn unconformably overlain by the Upper Triassic Jiapila (T_3j), Bolila (T_3b), Adula (T_3a) and Duogaila (T_3d) Formations. Sandstone and shale, locally interbedded with cupriferous sandstone, are the dominant rock types of the Jiapila Formation (>2000 m). The Bolila Formation consists chiefly of 480–1370 m of shallow-marine to littoral carbonate rocks. The Adula and Duogaila Formations are predominantly composed of a thick (800–2300 m) succession of limnic black shale and sandstone. The Jurassic to Cretaceous limnic sandstone and shale conformably overlie the Upper Triassic. Unconformably overlying all these units is the Lower Tertiary Gongjue Group, which consists of 3000 m of red conglomerate, sandstone and shale deposited in an intermontane basin.

Pre-Himalayan (Indosinian and Yanshanian) intrusive rocks in the Yulong belt range in composition from diorite through granodiorite to granite, and are chiefly associated with porphyrite-type Fe mineralization and skarn-type Cu–Fe–Pb–Zn mineralization. K–Ar isotopic ages of K-feldspar and biotite range from 230 to 85 Ma (*Tang* and *Luo*, 1995). Himalayan intrusive rocks are widespread in the belt and typically show a porphyritic texture. In the sections that follow, we mainly discuss the geologic and geochemical characteristics of the Himalayan porphyries, and interpret the relationship between the porphyries and associated Cu–Mo mineralization.

Himalayan porphyries

Porphyritic intrusions of the Himalayan epoch in the Yulong metallogenic belt are distributed in groups between the Ziga and the Tuoba-Mangkang faults (Fig. 1). From northwest to southeast are the Hengxingcuo porphyry group including the Xiariduo, Hengxingcuo and Yulong intrusions, the Zhanaga-Malasongduo porphyry group including the Zhanaga, Mangzong, Duoxiasongduo and Malasongduo intrusions, and the Gegonglong-Mamupu porphyry group including the Gegonglong, Jicuo, Riqu, Zengxi and Mamupu intrusions. These are multiphase, composite intrusions that typically range from monzogranitic porphyry and/or

biotite monzogranite, through quartz monzogranitic porphyry, granitic porphyry and/or albitophyre, to arizonite. The porphyries were mainly emplaced into Triassic and Lower Permian sedimentary-volcanic rocks, especially in Upper Triassic clastic rocks and carbonates. They occur as stocks, dikes, sills, apophyses, pipes or other irregular bodies, with outcrop areas commonly ranging from 0.1 to 1.5 km^2. Based upon 30 K–Ar dates for K-feldspar and biotite, the intrusion ages vary between 57 and 26 Ma (*Tang* and *Luo*, 1995; *Ma*, 1989, 1990). Four whole rock K–Ar ages reported by *Tang* and *Luo* (1995) range from 52 to 27 Ma. An U–Pb zircon age determination on the Angkelong intrusion gives an age of 41 Ma (*Ma*, 1989).

Rock types of the mineralized porphyries include mainly biotite monzogranitic porphyry and biotite syenogranitic porphyry, though beschtauite, quartz albitophyre and quartz syenodioritic porphyry are also present. Phenocrysts, commonly ranging from 0.5 to 10 mm in size comprise 35–50 vol% of the whole rock and consist of plagioclase (up to 30%), K-feldspar (up to 20%), quartz (1–12%), biotite (2–5%), hornblende (0–5%) and, rarely, sphene. The matrix, comprising 50 to 65 vol%, consists of K-feldspar, quartz and minor plagioclase. Magnetite, sphene, apatite, and zircon constitute accessory phases. Barren porphyries are indistinguishable from mineralized porphyries in both petrology and petrography. According to *Tang* and *Luo* (1995), Cu contents in phenocrystic K-feldspar (20–70 ppm), plagioclase (25–116 ppm) and biotite (40–218 ppm) from the mineralized porphyries are significantly higher than those from barren porphyries (2–6 ppm, 7–12 ppm and 14–42 ppm, respectively).

In this study, major and trace elements were determined for 15 porphyritic rocks from the Yulong intrusive complex. Major element oxides were analysed by X-ray fluorescence spectrometry at Chengdu University of Technology, China, following the methods of *Norrish* and *Hutton* (1969) and *Norrish* and *Chappell* (1977). Precision and accuracy for major elements are within 1–2%, except for P_2O_5 (5%). Trace elements, including rare earth elements, were analyzed by instrumental neutron activation analysis (INNA) at Chengdu University of Technology. Precision and accuracy of standards GSD11, P3C3, and GSOAu2, as determined by INNA, are within 5–10%. In addition, chemical data for 20 analyses from the other porphyry stocks in the Yulong belt are available from the literature (*Ma*, 1989, 1990; *Tang* and *Luo*, 1995) and are also included in the discussion. All the data are represented in Figs. 2 to 4. The comprehensive analytical dataset can be obtained from the first author upon request.

Geochemically, there are no significant correlations between SiO_2 and most of the major constituents of the porphyries. Most porphyritic rocks are calc-alkaline with alkalinity ratios (A.R.) ranging from 1.1 to 3.3 (Fig. 2a). They are characterized by relatively moderate contents of SiO_2 (typically 65–71 wt%) and high K_2O (4.0–8.1 wt%) and Na_2O (2.0–4.5 wt%) contents, and K_2O/Na_2O ratios (commonly 1.1–3.5, to a maximum of 31.9). Most samples are metaluminous to peraluminous with aluminum indices (molar ratios of $Al_2O_3/(CaO + Na_2O + K_2O)$) ranging from 0.8 to 2.6 (mostly below 1.1) and molar ratios of $Al_2O_3/(Na_2O + K_2O)$ ranging from 1.1 to 2.6 (Fig. 2b). The porphyries are of high K content (Fig. 2c) with no obvious differences observed between mineralized and barren porphyritic rocks in terms of major elements.

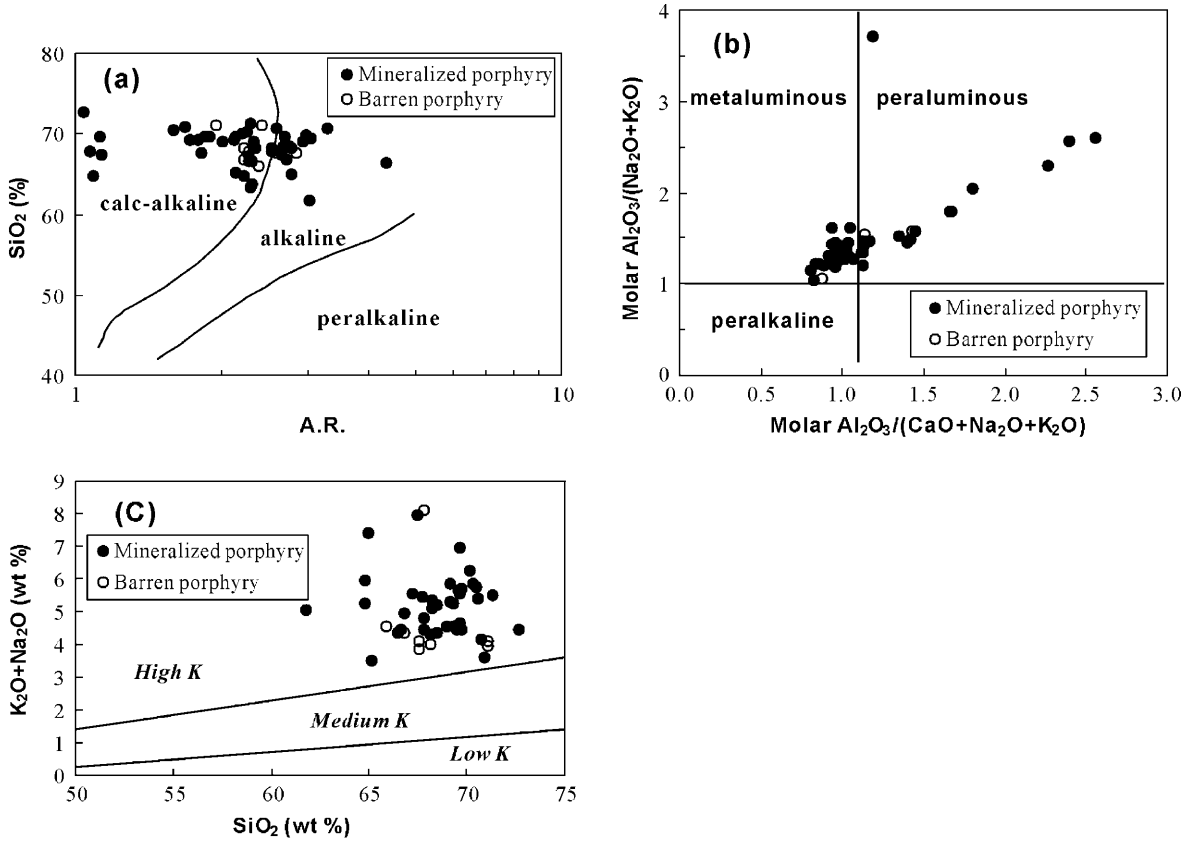

Fig. 2. Plots showing alkalinity (**a**), aluminum saturation (**b**), and the high K nature (**c**) of the porphyries in the Yulong belt

All the porphyritic rocks show similar primitive mantle-normalised trace element patterns, with depletion in Nb, Y and Ba (Fig. 3a, b). This pattern is similar to most modern subduction-related volcanic and plutonic rocks (*Wood* et al., 1979; *Briqueu* et al., 1984). The Nb depletion is typical of calc-alkaline magmatism from subduction-zone environments and may be an indicator of crustal involvement in magma processes (*Lan* et al., 1996; *Rollinson*, 1993). Both mineralized and barren porphyries have similar chondrite-normalized patterns (Fig. 3c,d) with high total REE abundances ($\Sigma\text{REE} = 277 \pm 72$ ppm), enriched LREE ($\Sigma\text{LREE}/\Sigma\text{HREE} = 20.9 \pm 2.4$), slightly negative Eu anomalies (Eu/Eu^* typically 0.75–0.98), and flat HREE distributions ($(\text{Gd}/\text{Yb})_n$ generally 1.6–3.0). It is apparent that fractional crystallization may not have played an important role in the generation of these porphyritic rocks.

In terms of ore-forming and associated elements, the mineralized porphyries have high contents of Cu (typically 170–2340 ppm), Mo (3.4–58.8 ppm), Au (4–30 ppb), Ag (1.5–2.7 ppm), F (1148–1758 ppm), B (commonly 15–55 ppm), S (0.04–0.9 wt%), and CO_2 (0.27–0.66 wt%). In contrast, the barren porphyries are low in concentrations of both ore-forming and associated elements, approximating to average crustal granitic rocks.

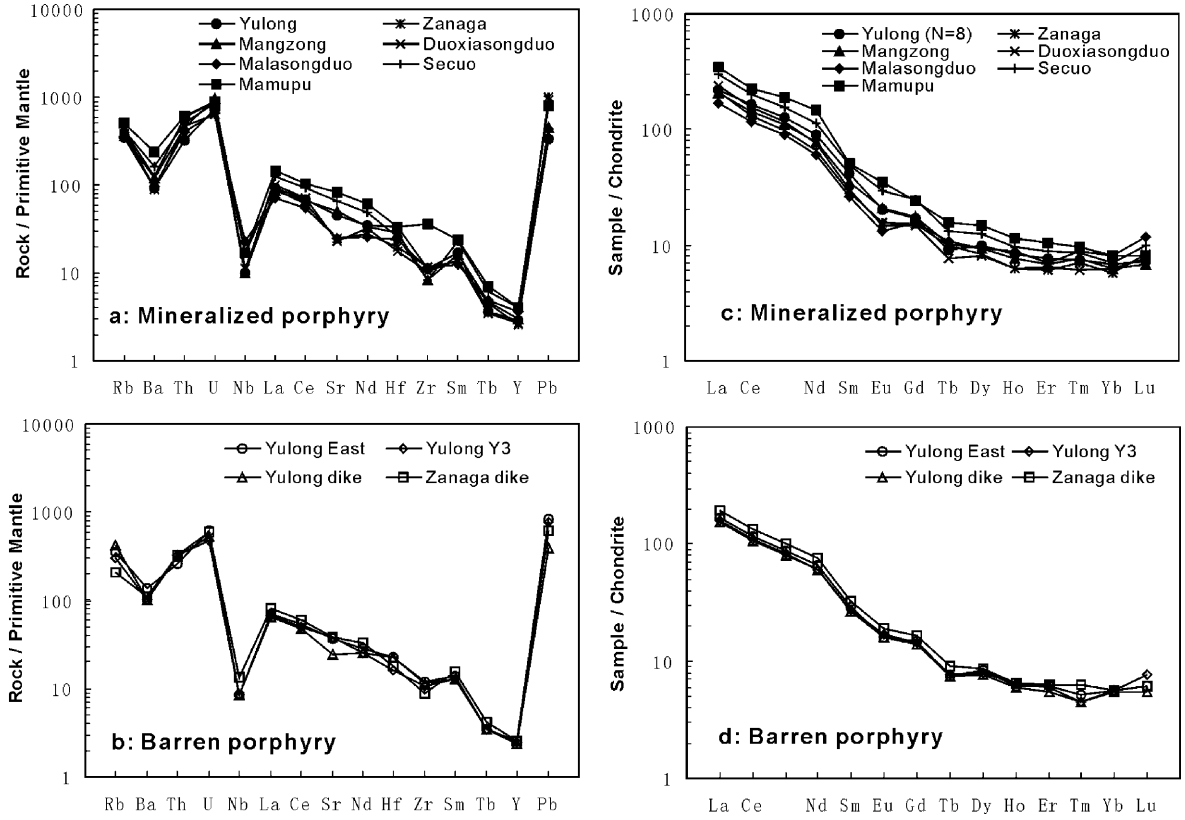

Fig. 3. Primitive mantle-normalized trace-element diagrams (**a**, **b**) and chondrite-normalized REE diagrams (**c**, **d**) for the Yulong porphyries. Note the similarity of various porphyritic intrusions and their identical depletion in Nb, Y and Ba

Geochemical and petrographic data presented in this study suggest that most porphyritic rocks in the Yulong belt exhibit characteristics of I-type granites with aluminum indices mostly below 1.1, high contents of normative magnetite (1–2%; *Tang* and *Luo*, 1995), high X_{Mg}/X_{Fe} values of biotite (1.9–3.1; *Tang* and *Luo*, 1995), and low initial ratios of $^{87}Sr/^{86}Sr$ (0.706–0.708; *Ma*, 1990). On the FeO^*–MgO–Al_2O_3 biotite discrimination diagram of *Abdel-Rahman* (1994), the porphyries show characteristics of orogenic, subduction-related, calc-alkaline suites including I-type granites (Fig. 4a). On the discrimination diagram of Rb versus Y + Nb of *Pearce* et al. (1984), they straddle the border of syn-collisional granites (syn-COLG) and volcanic arc granites (VAG), but most plot in the syn-COLG field (Fig. 4b). It is thus suggested that the magmatic evolution of the porphyries in the Yulong ore belt may have developed in two stages. During the Mesozoic time, the westward subduction of the Paleo-Tethyan oceanic crust beneath the Qiangtang-Changdu block, along the Jinshajiang suture zone, resulted in the partial melting of lower crust and the generation of felsic magmas. Later during the Himalayan orogeny, the continent–continent collision between the Indian block and Eurasia triggered the reactivation of the Paleo-Tethyan subduction zone and the emplacement of the syn-collisional subvolcanic intrusions.

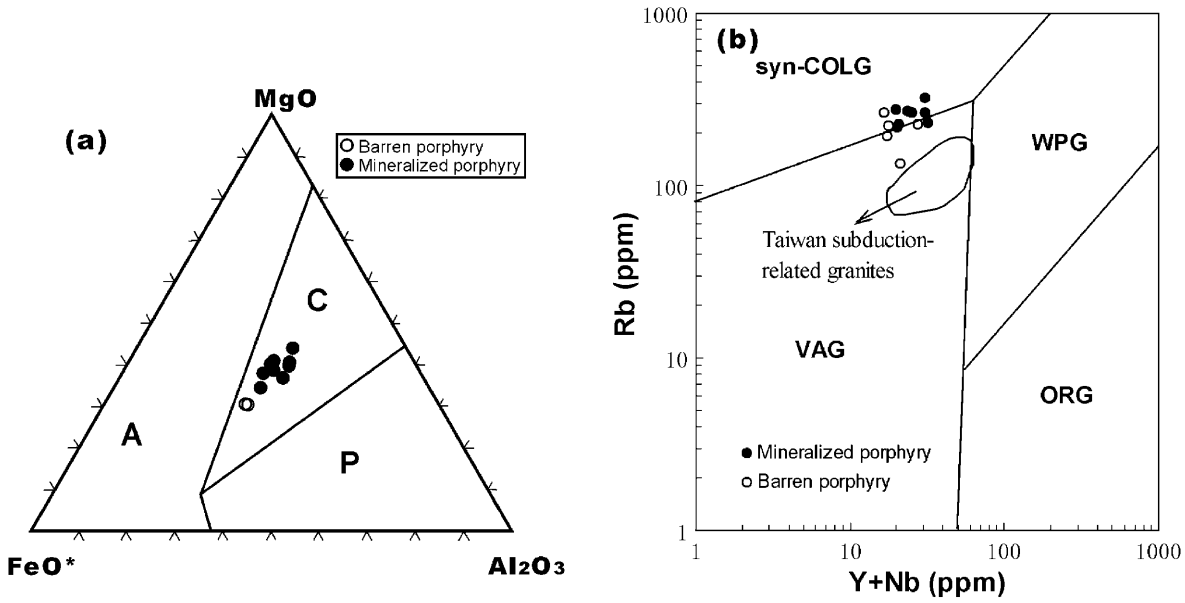

Fig. 4. **a** FeO^*–MgO–Al_2O_3 biotite discriminant diagram for the Yulong porphyries. Data from *Tang* and *Luo* (1995). A – Anorogenic extensional-related alkaline suites including A-type granites; C – Orogenic subduction-related calc-alkaline suites including I-type granites; P – Peraluminous suites including collisional and S-type granites (*Abdel-Rahman*, 1994). **b** Rb vs Y + Nb discrimination diagram for the Yulong porphyries. Also shown is the composition of Taiwan subduction-related granites (*Lan* et al., 1996). Fields for syn-collisional granites (syn-COLG), within-plate granites (WPG), volcanic-arc granites (VAG) and ocean-ridge granites (ORG) after *Pearce* et al. (1984)

Alteration and mineralization

Within the Yulong subvolcanic belt, a number of porphyry stocks bear typical porphyry style copper–molybdenum alteration and mineralization. The most prominent porphyry Co–Mo deposits include Yulong, Malasongduo, Duoxiasongduo, Mangzong and Zhanaga, of which Yulong is one of the largest porphyry Cu (Mo) deposits in China with approximately 8×10^6 tons of contained Cu metal.

Yulong porphyry Cu–Mo deposit

The Yulong biotite–monzogranitic porphyry was emplaced into a sequence of sedimentary rocks of Upper Triassic age, consisting of lower units of mudrock and siltstone intercalated with quartzite (Jiapila Formation, T_3j) and upper units of limestone, argillaceous limestone, and calcareous sandstone (Bolila Formation, T_3b; Fig. 5a). The intrusion occurs as a pipelike, mineralized subvolcanic body with a surface area of 0.64 km^2 and a vertical extent of at least 850 m. The contacts with the wall rocks are steep and discordant. K–Ar isotopic dating on K-feldspar and biotite gives ages of 38–58 Ma (*Tang* and *Luo*, 1995; *Ma*, 1989, 1990).

The Yulong intrusive body exhibits strong hydrothermal alteration that forms more or less concentric zones extending outward from the inner part of the intrusion. These zones vary from a potassic core, through a phyllic (quartz–sericite–pyrite)

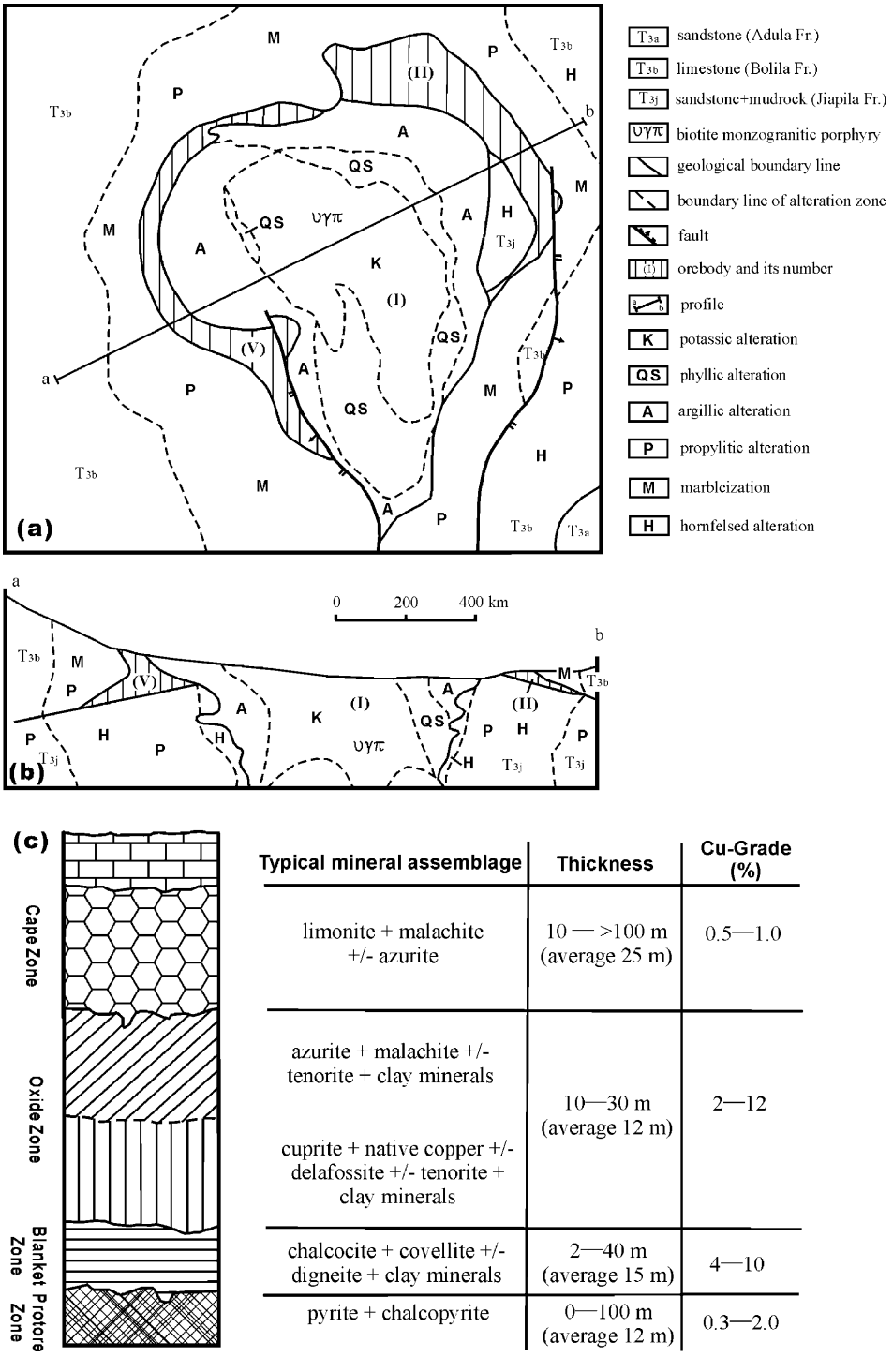

Typical mineral assemblage	Thickness	Cu-Grade (%)
limonite + malachite +/- azurite	10 — >100 m (average 25 m)	0.5—1.0
azurite + malachite +/- tenorite + clay minerals	10—30 m (average 12 m)	2—12
cuprite + native copper +/- delafossite +/- tenorite + clay minerals		
chalcocite + covellite +/- digneite + clay minerals	2—40 m (average 15 m)	4—10
pyrite + chalcopyrite	0—100 m (average 12 m)	0.3—2.0

Fig. 5. Simplified geologic map of the Yulong porphyry Cu–Mo deposit showing the alteration–mineralization patterns (**a**, **b**; modified after *Tang* and *Luo*, 1995) and schematic profile showing relation between the cap zone, oxide zone, enrichment blanket and protore of the oxidized skarn-type orebody (**c**)

zone, an argillic zone, to a propylitic zone (Fig. 5a,b). This pattern reflects the typical alteration style of porphyry type Cu (Mo) deposits (e.g., *Lowell* and *Guilbert*, 1970; *Rose*, 1970; *Hunt*, 1991; *Frezzotti* et al., 1992; *Titley*, 1993; *Beane* and *Bodnar*, 1995; *Hezarkhani* and *Williams-Jones*, 1998; *Hedenquist* et al., 1998; *Selby* et al., 2000).

The potassic alteration zone is characterized by the pervasive alteration of plagioclase to orthoclase, hornblende and primary biotite to secondary biotite, and the formation of microveinlet fillings of quartz + K-feldspar + biotite ± sericite ± sulfides. The alteration was accompanied by a small amount of disseminated and veinlet-type Cu–Mo sulfide mineralization. The typical ratio of pyrite (Py)/chalcopyrite (Cpy)/molybdenite (Mo) is about 35:70:1. During this stage, metasomatism and/or contact metamorphism in country rocks adjacent to the porphyry body produced andradite–diopside–idocrase exoskarns, quartz–plagioclase–biotite hornfels, and marbles. Disseminated and locally massive pyrite, chalcopyrite, magnetite and pyrrhotite occur in the skarns. Pyrite–chalcopyrite veinlets and disseminations also occur in the hornfels and marbles.

The phyllic zone surrounds and overlaps the potassic zone. Contacts between the phyllic and potassic zones are gradational. This alteration is characterized by the replacement of almost all rock-forming silicates by sericite and quartz. Pyrite is the most common sulfide, whereas chalcopyrite and molybdenite are present in subordinate amounts (Py/Cpy/Mo ~ 40:20:1). Sulfide minerals comprises 3–5 vol% of the altered rock. The phyllic alteration is confined to a major stage during which most of the Cu and Mo was deposited.

Argillic alteration is well developed in the Yulong deposit. It is characterized by the replacement of biotite and feldspar by clay minerals and the formation of comby quartz–sulfide veins. XRD analyses indicate that halloysite and kaolinite are the dominant clay minerals, although montmorillonite, illite and chlorite are also present. Locally, at the contact between the intrusion and wall rocks where cleavages are well developed, advanced argillic alteration is manifested by the formation of kaolinite–halloysite and varying amounts of allophanite, alunite, and amorphous silica. The main ore mineral assemblage comprises pyrite, chalcocite and covellite. These occurr within microfractures as rims around the former ore minerals and almost completely replace chalcopyrite, which is observed only as sparse relics. The presence of chalcocite and covellite replacing chalcopyrite in the primary argillic zone and the structurally-controlled nature of the advanced argillic alteration suggest a later oxidation and supergene process.

Propylitic alteration forms a wide halo in the country rocks and overprints the other alteration zones. The main assemblage consists of epidote, chlorite, albite, calcite, and pyrite that occurs as fine-grained aggregates or as veinlets. Pyrite is abundant and chalcopyrite is rare (Py/Cpy ~ 5–10:1).

Porphyry-type (orebody I) and skarn-type (orebody II and V) ores constitute two major mineralization styles in the Yulong deposit (Fig. 5a,b). Above an elevation of 4700 m, the whole porphyritic body is mineralized. Ore mineral assemblages occur in disseminated or stockwork forms. Mineral zoning is characterized by increasing Cu/Mo inward and downward. The skarn-type orebodies occur within 200 m of the contact and form a wedge-shaped ring of andradite–diopside–idocrase exoskarns that decrease in thickness outward. The inner zone

near the contact is mainly composed of coarse-grained anhydrous skarn minerals (andradite + diopside + idocrase) and 5–8% ore minerals (pyrite + chalcopyrite + magnetite + pyrrhotite ± scheelite ± bismuthinite). Towards the outer zone, the content of ore minerals decreases (3–5%) and the anhydrous skarn assemblages are gradually replaced by hydrous minerals such as tremolite, actinolite, epidote and chlorite. The most prominent feature of the skarn-type orebodies is extensively developed leaching, oxidation and secondary enrichment. The richest Cu ores (up to 38% Cu) are derived from the zone of secondary enrichment. These processes are especially well manifested in the orebody II, where almost all the primary skarn minerals have been destroyed and replaced by clay minerals (halloysite + kaolinite + montmorillonite), while sulfides have been replaced by oxides, carbonates, secondary sulfides and native copper. In a typical profile of the oxidized orebody II (Fig. 5c), a leached cap of limonite and malachite with less than 1.0% Cu is followed by an enrichment zone of azurite + cuprite + native copper ± delafossite ± tenorite ± malachite (generally 2–12% Cu), and finally an enrichment zone of chalcocite + covellite ± digneite (4–10% Cu).

A fluid inclusion study was undertaken in order to estimate the spatial and temporal variations in temperature and composition of the hydrothermal fluids. Microthermometric measurements were performed on doubly polished sections using a TRL-02 heating–freezing stage at Chengdu University of Technology. Calibrations were made using organic standards with known melting points, and the accuracy was determined to be within 1 °C over the temperature range of this study.

Quartz from both mineralized porphyries and associated veins contains abundant fluid inclusions. They vary in size from 1 to 40 μm, with a large population around 5 to 15 μm. On the basis of room temperature phase relations, four major types of fluid inclusions are distinguished. Type VL are vapor-rich, two-phase (vapor + liquid) inclusions. The vapor bubbles usually exceed 80 percent of the total volume. Most of the VL inclusions are primary with rounded or negative crystal shapes. Type LV inclusions are liquid-rich, two-phase (liquid + vapor) inclusions, which are characterized by a vapor bubble of variable size, but never exceed 20 percent by volume of the whole inclusion. Both primary (occurring in clusters with rounded or negative crystal shapes) and secondary (occurring along microfissures with oblate or irregular shapes) LV inclusions were identified. Type LVS inclusions are multiphase and of primary origin. They consist of liquid + vapor + solid daughter minerals. Halite, sylvite and anhydrite are the common daughter minerals, although chalcopyrite and molybdenite are also present. The volume of the solid phases is typically <35 percent of the inclusions and the bubble volumes range between 5 and 50 percent. Type LVC inclusions consist of liquid H_2O and CO_2, and vapor CO_2. The volume of liquid and vapor CO_2 varies between 20 and 80 percent of the inclusions.

The spatial distribution of fluid inclusion indicates that different alteration–mineralization zones have different fluid inclusion populations, reflecting the evolution of hydrothermal fluids. Quartz within the potassic zone is characterized by having abundant VL and LVS inclusions, although LV inclusions are also present. Homogenization temperatures (T_h) of these inclusions range between 660° and 420 °C, (typically 600°– 420 °C, Fig. 6a). In the highly mineralized phyllic zone,

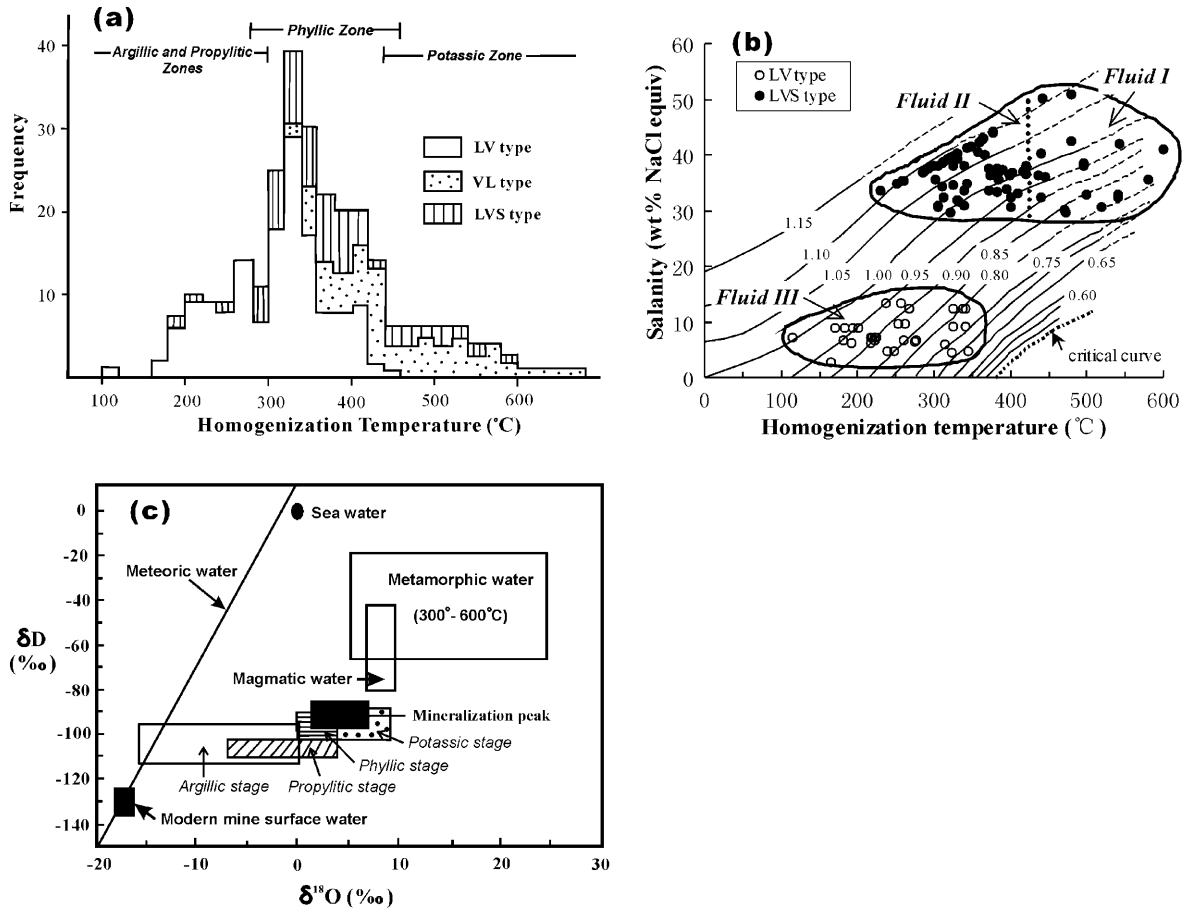

Fig. 6. **a** Histogram of homogenization temperatures for LV, VL, and LVS fluid inclusions from mineralized quartz veins in the Yulong Cu–Mo deposit. **b** Diagram showing homogenization temperature (°C) – salinity (wt% NaCl equiv) – density (g/cm^3) relationship in the NaCl–H_2O system (after *Ahmad* and *Rose*, 1980) for LV and LVS fluid inclusions in the Yulong deposit. Different subsets of inclusions outline three distinct fluid generations (see text for explanation). **c** Plot of δD vs δ^{18}O for the hydrothermal fluids in the Yulong deposit (data after *Rui* et al., 1984; *Zhang*, 1985; *Ma*, 1990). Meteoric water line after *Craig* (1961). Compositions of magmatic waters and metamorphic waters after *Taylor* (1974) and *Zhang* (1985)

all fluid inclusion types are present. The coexistence of types LV, VL, LVS and LVC inclusions and the observation that the coexisting LV, VL and LVS inclusions homogenized to a vapor or liquid over a similar temperature range (460°–230 °C, mostly 420°–280 °C) suggest boiling of the hydrothermal fluids during this stage. In the shallow parts of the system where argillic and propylitic alterations are best developed, type LV inclusions become increasingly important and volumetrically dominant (up to 80% of the inclusions). They homogenize to a liquid in a typical temperature range of 300°–160 °C.

The salinities presented in Fig. 6b were calculated based on final ice-melting temperatures (T_{fm}) for type LV inclusions and halite dissolution temperatures (T_{hH}) for type LVS inclusions (*Potter* et al., 1978; *Bodnar*, 1994; *Sterner* et al., 1988). Three distinct fluid populations may be outlined. Fluid I is recorded by type LVS inclusions in quartz typically from the potassic zone. It is characterized by high temperatures (Th = 600°–420 °C) and high salinities (30–51 wt% NaCl equiv), with corresponding densities of 0.80–1.10 g/cm^3. This fluid represents the earliest fluid in the hydrothermal history of the complex. Fluid II is recorded by type LVS inclusions from the phyllic alteration–mineralization zone. Evidence of extensive boiling of this fluid indicates that it represents an unmixed fluid evolved from the fluid I. Boiling must have continued for a long T-interval, probably down to 230 °C. However, the small change in salinity (30–44 wt% NaCl equiv) and density (0.90–1.10 g/cm^3) compared to Fluid I suggests a rapid drop in both temperature and pressure. Fluid III is recorded by type LV inclusions in quartz mostly from the argillic and propylitic zones. It is characterized by a wide temperature range (345°–115 °C) and low salt content (3–13 wt% NaCl equiv), with corresponding densities of 0.95–1.00 g/cm^3. It is possibly related to the final stage of hydrothermal evolution and represents a mixed fluid of magmatic and meteoric waters.

Sulfur isotope analyses were performed on 13 pyrite, chalcopyrite and molybdenite samples (Table 1). Mineral separation was by handpicking under a binocular microscope. The analyses were performed at the Isotope Laboratory at the Yichang

Table 1. *Sulfur isotope data of sulfides from the Yulong deposit*

Sample no.	Ore/Rock	Mineral	$^{34}S_{CDT}$ (‰)			Data source
			Value	Range	Average	
	porphyritic ore	pyrite		− 0.5 to 3.8 (23)	2.4	1
	porphyritic ore	chalcopyrite		0.9 to 2.8 (9)	2.1	1
	porphyritic ore	molybdenite		2.4 to 2.8 (2)	2.6	1
	skarn ore	pyrite		1.4 to 2.3 (4)	2.1	1
ZK32-11	skarn ore	pyrite	2.1			2
ZK51-8	skarn ore	pyrite	1.8			2
ZK32-W5	skarn ore	pyrite	2.3			2
ZK34-10	skarn ore	pyrite	6.0			2
ZK51-10	skarn ore	pyrite	2.4			2
ZK55-9	skarn ore	pyrite	1.5			2
ZK59-10	skarn ore	pyrite	1.4			2
ZK1808-14	skarn ore	pyrite	1.4			2
ZK1808-41	skarn ore	pyrite	1.4			2
ZK36-5	skarn ore	pyrite	2.9			2
ZK59-W1	skarn ore	molybdenite	− 1.3			2
	hornfels	pyrite		− 21.4 to 1.1 (14)	0.1	1
ZK44-6	hornfels	pyrite	1.1			2
ZK59-14	hornfels	pyrite	2.3			2
	mineralized marble			1.4 to 13.8 (4)	7.3	1

Number of measurements is given in parentheses. Data source: *1 Rui* et al. (1984); *2* this study

Institute of Geology and Mineral Resources, Ministry of Land and Resources. The values are precise to a level of 0.1 per mil. Also included in Table 1 are sulfur isotope data reported by *Rui* et al. (1984).

A magmatic origin of the sulfur is suggested by the $\delta^{34}S$ values of disseminated and vein-related pyrite, chalcopyrite and molybdenite in porphyry-type ores, which range from -0.5 to 3.8 per mil. Sulfur isotopes are relatively scattered in the sulfides from skarn-type ores ($\delta^{34}S = -1.3 \sim 6.0‰$), hornfels ($\delta^{34}S = -21.4 \sim 2.3‰$) and mineralized marbles ($\delta^{34}S = +1.4 \sim +13.8‰$), reflecting the increasing influence of sedimentary sulfur outward from the porphyry stock.

Rui et al. (1984), *Zhang* (1985) and *Ma* (1990) reported hydrogen and oxygen isotope data from fluid inclusions in quartz from different alteration zones. These data are reproduced in Fig. 6c. The early hydrothermal fluids responsible for the potassic alteration vary in $\delta^{18}O$ from 3.2 to 8.5‰ and δD from -102 to $-88‰$ are similar to the primary magmatic waters isotopically equilibrated with Au–Cu series granites ($\delta^{18}O = 6.0 \sim 9.0‰$, $\delta D = -110 \sim -65‰$; *Zhang*, 1985). They were succeeded by isotopically light waters, from the phyllic alteration stage ($\delta^{18}O = 0.7 \sim 3.8‰$, $\delta D = -102 \sim -89‰$) to the propylitic alteration stage ($\delta^{18}O = -6.8 \sim 3.3‰$, $\delta D = -110 \sim -102‰$) and to the advanced argillic alteration stage ($\delta^{18}O = -16.2 \sim 0.6‰$, $\delta D = -112 \sim -97‰$), reflecting increasing addition of meteoric-derived convective waters.

Other porphyry Cu–Mo deposits

Other porphyry Cu–Mo deposits in the Yulong ore belt are broadly similar to the Yulong deposit in alteration and mineralization styles. The Malasongduo biotite monzogranitic porphyry stock, with K–Ar ages (K-feldspar and biotite; *Tang* and *Luo*, 1995) of 32–49 Ma, was intruded into Lower Triassic rhyolite and tuff (Malasongduo Formation, T_1m; Fig. 7a). The mineralization, with average grades of 0.3–0.6% Cu and 0.014% Mo, occurs within and around the porphyry body. From the intrusive outward, a distinct mineralization zoning pattern consisting of Cu, Cu + Mo, and Ag + Pb + Zn, with increasing pyrite/chalcopyrite ratios, is present. The primary ore mineral is chalcopyrite; other ore minerals include molybdenite, sphalerite, galena and associated Au and Ag. Oxidation and secondary enrichment characterized by the presence of hematite + malachite ± covellite ± chalcocite ± delafossite ± native copper, are poorly developed and only locally seen in the uppermost parts of the orebody.

In the Duoxiasongduo Cu–Mo deposit (Fig. 7b), the mineralization has average grade of 0.38% Cu and 0.02% Mo and occurs within and around the south contact of a monzogranitic porphyry stock (28–31 Ma, K–Ar ages of K-feldspar; *Tang* and *Luo*, 1995) that was emplaced into sandstone, siltstone and mudstone of the lower part of the Upper Triassic Jiapila Formation (T_3j^1). The molybdenum content increases downward. Sulfide–oxide species include pyrite, chalcopyrite, molybdenite and specularite. Native gold is also present in the specularite and quartz–sulfide veins.

In the Mangzong Cu–(Mo) deposit (Fig. 8a), an Oligocene composite stock, which consists of early monzogranitic and quartz monzonitic porphyry, followed by granitic porphyry and late dioritic porphyrite, intruded into Lower Permian

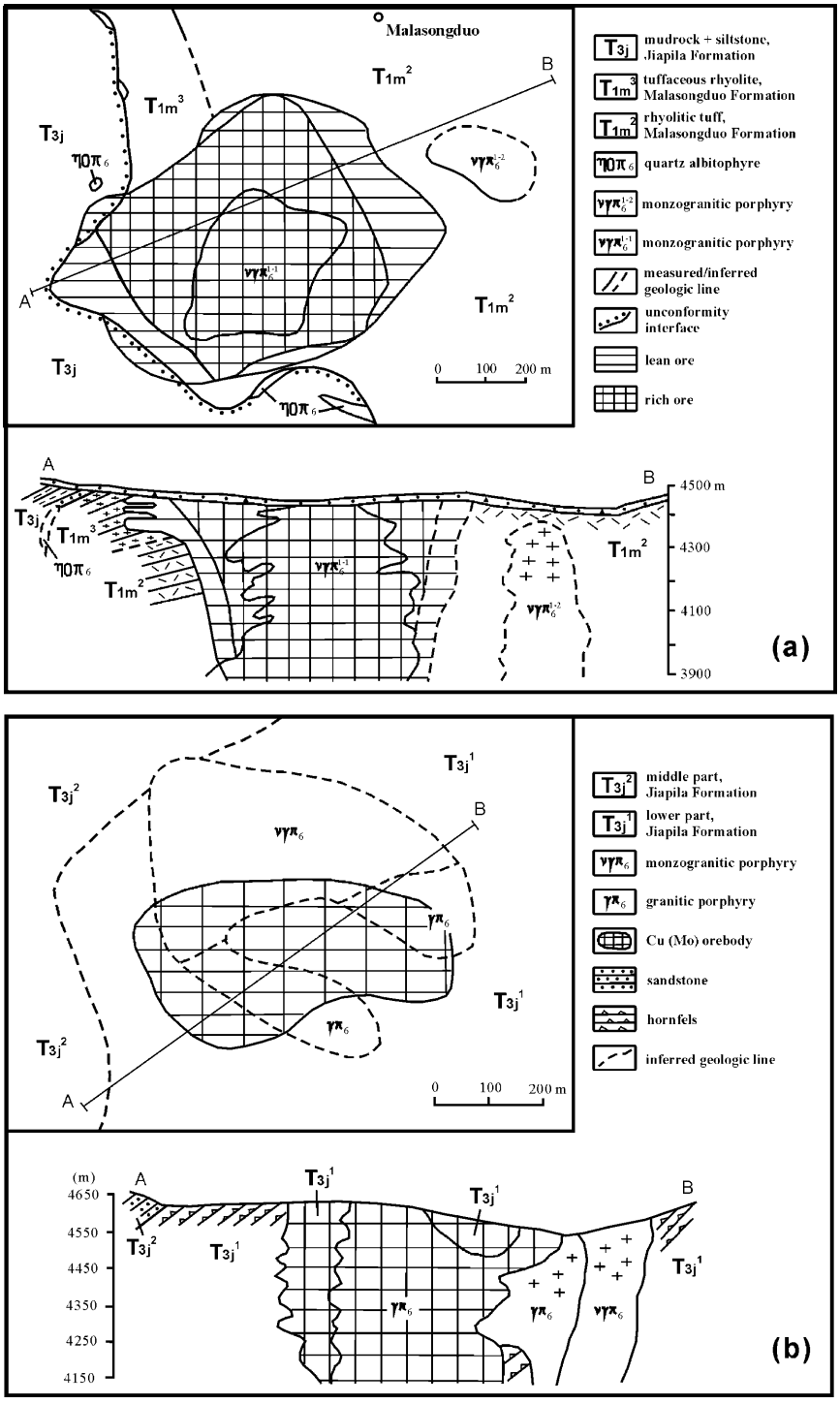

Fig. 7. Schematic geologic maps of the Malasongduo (**a**) and Duoxiasongduo (**b**) Cu–Mo deposits (simplified after *Tang* and *Luo*, 1995)

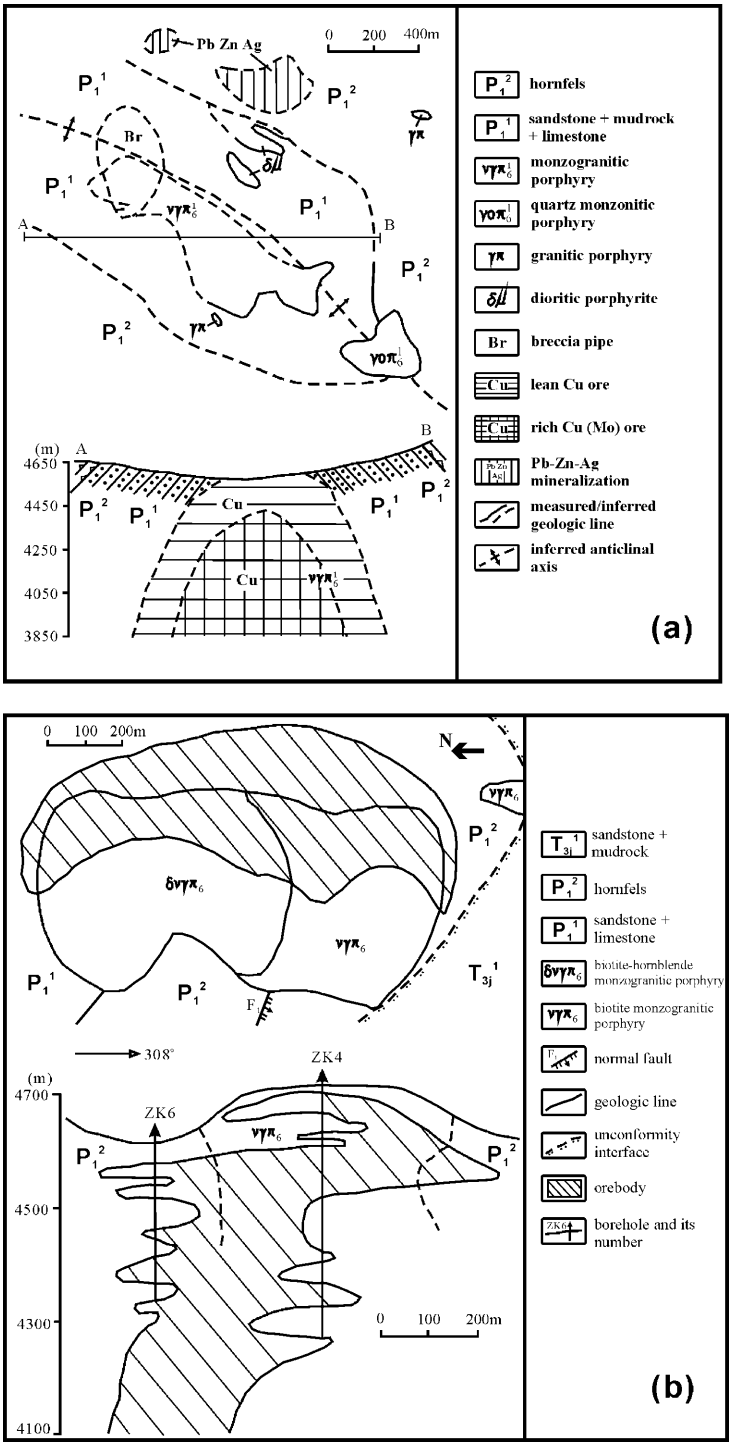

Fig. 8. Schematic geologic maps of the Mangzong (**a**) and Zhanaga (**b**) Cu–Mo deposits (simplified after *Tang* and *Luo*, 1995)

sandstone and mudrock interbedded with limestone. The mineralization forms a concentric shell centered on the early monzogranitic porphyry body. Ore mineral paragenesis indicates an early quartz + pyrite + chalcopyrite ± molybdenite stage and a late stage containing sphalerite + galena + pyrite ± specularite. Both Mo contents and chalcopyrite/pyrite ratios decrease with distance from the intrusive.

The Zhanaga composite stock (35–36 Ma, K–Ar ages of K-feldspar; *Tang* and *Luo*, 1995), consisting of biotite–hornblende monzogranitic porphyry and biotite monzogranitic porphyry, was emplaced into Lower Permian sandstone and limestone and Upper Triassic clastic rocks (Jiapila Formation, T_3j; Fig. 8b). The mineralization has an average grade of 0.36% Cu and 0.02% Mo, and occurs within the potassic and phyllic alteration zones at the east contact of the stock. Pyrite, chalcopyrite and molybdenite are the common sulfides in the ore.

Concluding remarks

The porphyry-related copper–molybdenum deposits in the Yulong ore belt of eastern Tibet are genetically associated with magmatic activity during the Himalayan epoch. The Himalayan intrusions form a 400 km long and 35–70 km wide belt of porphyritic rocks, which were mainly emplaced into Triassic and Lower Permian sedimentary-volcanic rocks in a reactivated continental island arc tectonic setting following continent–continent collision between the Indian plate and Eurasia.

The intrusive porphyritic rocks are typical I-type granitoids of predominantly granitic composition and represent a high-K calc-alkaline suite. Except for remarkably higher contents of ore-forming elements (Cu, Mo, Au, Ag) and associated elements (F, B, S, CO_2) in mineralized porphyries, no obvious differences exist between mineralized and barren porphyries in terms of major oxide, trace element and initial Sr isotope compositions, thus suggesting a common and/or similar magma source.

The porphyry copper–molybdenum deposits in the Yulong belt, including Yulong, Malasongduo, Duoxiasongduo, Mangzong and Zhanaga, exhibit broadly similar features in alteration and mineralization. At Yulong, the hydrothermal alteration forms concentric zones, extending from a potassic core outward to a phyllic zone, an argillic zone, and a propylitic zone. In country rocks adjacent to the porphyry body, metasomatism and contact metamorphism represented by andradite–diopside–idocrase exoskarns, quartz–plagioclase–biotite hornfels and marbles are well developed. The phyllic alteration is confined to a major stage during which most of the Cu and Mo were deposited, though a small amount of disseminated and veinlet Cu–Mo sulfide mineralization is associated with the potassic alteration and contact metasomatism. Porphyry-type and skarn-type ores constitute two major mineralization styles in the Yulong deposit, while in the other deposits the porphyry-type mineralization predominates.

The action of magmatic and meteoric fluids in porphyry systems produced the alteration and mineralization patterns of the deposits, which depend on the nature of the fluids, wall rock and intrusive compositions, and probably the permeability of porphyry systems. The study of fluid inclusions at Yulong indicates that there are three types of fluids that have been involved in the alteration–mineralization processes: (1) early high temperature (660–420 °C) and high salinity (30–51 wt%

NaCl equiv) fluids responsible for potassic alteration and the earliest disseminated and/or veinlet Cu–Mo sulfide mineralization; (2) intermediate unmixed fluids corresponding to phyllic alteration and most Cu–Mo sulfide mineralization, with salinities of 30–50 wt% NaCl equiv and homogenization temperatures of 460–280 °C; and (3) late low to moderate temperature (300–160 °C) and low salinity (6–13 wt% NaCl equiv) fluids, responsible for argillic and propylitic alteration. Hydrogen and oxygen isotopic studies show that the early hydrothermal fluids were of magmatic origin and were succeeded by increasing amounts of meteoric-derived convective waters. Sulfur isotopes support a magmatic source for the sulfur of the early disseminated and veinlet mineralization, with an increasing addition of sedimentary sulfur outward from the porphyry stock.

Acknowledgements

This paper was presented at the 16th Himalaya-Karakorum-Tibet Workshop, Schloss Seggan, near Graz, Austria, in April, 2001. We wish to thank all personnel of the 6th Geological Team, Bureau of Geology and Mineral Resources of Tibet for their support during the field work, with special mention for geologists *W. Huang*, *D. Q. Xia*, *D. K. Su*, *Y. T. Mei*, *J. S. Zhang*, and *Q. Z. Zhang*. We are grateful to Prof. *M. H. Zheng* for constructive discussions and reviews of early drafts of the manuscript, and *B. H. Li* for assistance in the fluid inclusion study. Critical reviews by Drs. *D. Arne* and *D. Jessey* have greatly improved the manuscript. We acknowledge the insightful handling from Dr. *K. Stüwe*. The research was supported by the National Natural Science Foundation of China (NSFC) under the grant of 49872038, the Chinese Academy of Sciences under a special grant for young national scientists, and the Ministry of Science and Technology of China under the 973 National Basic Research Priorities Programme.

References

Abdel-Rahman AM (1994) Nature of biotites from alkaline, calc-alkaline, and peraluminous magmas. J Petrol 35: 525–541

Ahmad SN, Rose AW (1980) Fluid inclusions in porphyry and skarn ore at Santa Kita, New Mexico. Econ Geol 75: 229–250

Beane RE, Bodnar RJ (1995) Hydrothermal fluids and hydrothermal alteration in porphyry copper deposits. In: *Pierce FW, Bohm JG* (eds) Porphyry copper deposits of the American Cordillera. Arizona Geological Society Digest 20, Tucson, pp 83–93

Bodnar RJ (1994) Synthetic fluid inclusions XII. The system H_2O–NaCl: experimental determination of the liquidus and isochores for a 40 wt% H_2O–NaCl solution. Geochim Cosmochim Acta 58: 1053–1063

Briqueu L, *Bougault H*, *Joron JL* (1984) Quantification of Nb, Ta, Ti and V anomalies in magmas associated with subduction zones – petrogenetic implications. Earth Planet Sci Lett 68: 297–308

Craig H (1961) Isotopic variations in meteoric waters. Science 133: 1702–1703

Frezzotti ML, Ghezzo C, Stefanini B (1992) The Calabona intrusive complex (Sardinia, Italy): evidence for a porphyry copper system. Econ Geol 87: 425–436

Gu XX, Tang JX, Wang CS (2000) Porphyry and skarn Cu–Mo–Pb–Zn–Ag–Au metallogeny of the Gangdise plutonic–volcanic arc, Tibet. Earth Science Frontiers 7 [Suppl]: 430

Hao ZW, *Yu RL* (1983) The Kunlun-Bayan Har sea and its relation to evolution of Tethys. In: *CGQXP Editorial Committee* (ed) Contribution to the geology of the Qinghai-Xizang

(Tibet) plateau. Geological Publishing House, Beijing, pp 25–41 (in Chinese with English abstract)

Hedenquist JW, Arribas A, Reynolds TJ (1998) Evolution of an intrusion-centered hydrothermal system: Far Southeast-Lepanto porphyry and epithermal Cu–Au deposits, Philippines. Econ Geol 93: 373–404

Hezarkhani A, Williams-Jones AE (1998) Controls of alteration and mineralization in the Sungun porphyry copper deposit, Iran: evidence from fluid inclusions and stable isotopes. Econ Geol 93: 651–670

Hunt JP (1991) Porphyry copper deposits. Econ Geol Monogr 8: 192–206

Lan CY, Jahn BM, Mertzman SA, Wu TW (1996) Subduction-related granitic rocks of Taiwan. J Southeast Asian Earth Sci 14: 11–28

Lowell JD, Guilbert JM (1970) Lateral and vertical alteration–mineralization zoning in porphyry ore deposits. Econ Geol 65: 373–408

Ma HW (1989) On the intrusive ages of magmas in the Yulong porphyry copper belt, eastern Tibet. Geochimica 10: 210–215 (in Chinese)

Ma HW (1990) Granitoid and mineralization in the Yulong porphyry copper ore belt, Tibet. China University of Geosciences Press, Beijing, 158 pp (in Chinese with English abstract)

Norrish K, Chappell BW (1977) X-ray fluorescence spectrometry. In: *Zussman J* (ed) Physical methods in determinative mineralogy. Academic Press, New York, pp 235–237, 257–262

Norrish K, Hutton JT (1969) An accurate X-ray spectrographic method for the analysis of a wide range of geological samples. Geochim Cosmochim Acta 33: 431–454

Pearce JA, Harris NBW, Tindle AG (1984) Trace element discrimination diagram for the tectonic interpretation of granitic rocks. J Petrol 25: 956–983

Potter RW, Clynne MA, Brown DL (1978) Freezing point depression of aqueous sodium chloride solutions. Econ Geol 73: 284–285

Rollinson HR (1993) Using geochemical data: evaluation, presentation, interpretation. Longman Scientific & Technical, Singapore, 352 pp

Rose AW (1970) Zonal relations of wallrock alteration and sulfide distribution at porphyry copper deposits. Econ Geol 65: 920–936

Rui ZY, Huang ZK, Qi GM (1984) Porphyry copper (molybdenum) deposits in China. Geological Publishing House, Beijing, 350 pp (in Chinese with English abstract)

Selby D, Nesbitt BE, Muehlenbachs K, Prochaska W (2000) Hydrothermal alteration and fluid chemistry of the Endako porphyry molybdenum deposit, British Columbia. Econ Geol 95: 183–202

Sterner SM, Hall DL, Bodnar RJ (1988) Synthetic fluid inclusions V. Solubility relations in the system NaCl–KCl–H_2O under vapor-saturated conditions. Geochim Cosmochim Acta 52: 989–1005

Tang RL, Luo HS (1995) The geology of Yulong porphyry copper (molybdenum) ore belt, Xizang (Tibet). Geological Publishing House, Beijing, 320 pp (in Chinese with English abstract)

Taylor HP Jr (1974) The application of oxygen and hydrogen isotope studies to problems of hydrothermal alteration and ore deposition. Econ Geol 69: 843–883

Titley SR (1993) Characteristics of porphyry copper occurrence in the American Southeast. Geol Assoc Can Spec Paper 40: 433–464

Wood DA, Joron JL, Treuil M (1979) A reappraisal of the use of trace elements to classify and discriminate between magma series erupted in different tectonic settings. Earth Planet Sci Lett 45: 326–336

Zhang LG (1985) The application of stable isotope to geology – the hydrothermal mineralization of metal activation and its prospecting. Shanxi Publishing House of Science and Technology, Xi'an, 267 pp (in Chinese with English abstract)

Zhang QW, Ai CX, Li TZ, Yu XJ (1983) Evolution of the trench-arc-basin tectonic system in the middle belts of Sanjiang. In: *CGQXP Editorial Committee* (ed) Contribution to the geology of the Qinghai-Xizang (Tibet) plateau. Geological Publishing House, Beijing, pp 95–104 (in Chinese with English abstract)

Authors' addresses: *X. X. Gu*, Institute of Geochemistry, Chinese Academy of Sciences, Guiyang 550002, P.R. China, e-mail: xuexiang_gu@263.net; *J. X. Tang*, *C. S. Wang*, *J. P. Chen*, and *B. B. He*, Chengdu University of Technology, Chengdu 610059, P.R. China, e-mail: tjx@cdut.edu.cn